

This is a self-archived version of an original article. This version may differ from the original in pagination and typographic details.

Author(s): Al-Majid, Abdullah M.; Soliman, Saied M.; Haukka, Matti; Ali, M.; Islam, Mohammad S.; Shaik, Mohammed R.; Barakat, Assem

Title: Design, Construction, and Characterization of a New Regioisomer and Diastereomer Material Based on the Spirooxindole Scaffold Incorporating a Sulphone Function

Year: 2020

Version: Published version

Copyright: © 2020 the Authors

Rights: CC BY 4.0


Rights url: <https://creativecommons.org/licenses/by/4.0/>

Please cite the original version:

Al-Majid, A. M., Soliman, S. M., Haukka, M., Ali, M., Islam, M. S., Shaik, M. R., & Barakat, A. (2020). Design, Construction, and Characterization of a New Regioisomer and Diastereomer Material Based on the Spirooxindole Scaffold Incorporating a Sulphone Function. *Symmetry*, 12(8), Article 1337. <https://doi.org/10.3390/sym12081337>

Article

Design, Construction, and Characterization of a New Regioisomer and Diastereomer Material Based on the Spirooxindole Scaffold Incorporating a Sulphone Function

Abdullah Mohammed Al-Majid ¹, Saied M. Soliman ², Matti Haukka ³, M. Ali ¹,
Mohammad Shahidul Islam ¹, Mohammed Rafi Shaik ¹ and Assem Barakat ^{1,2,*}

¹ Department of Chemistry, College of Science, King Saud University, P.O. Box 2455, Riyadh 11451, Saudi Arabia; amajid@ksu.edu.sa (A.M.A.-M.); maly.c@ksu.edu.sa (M.A.); mislam@ksu.edu.sa (M.S.I.); mrshaik@ksu.edu.sa (M.R.S.)

² Department of Chemistry, Faculty of Science, Alexandria University, P.O. Box 426, Ibrahimia, Alexandria 21321, Egypt; saied1soliman@yahoo.com or saeed.soliman@alexu.edu.eg

³ Department of Chemistry, University of Jyväskylä, P.O. Box 35, FI-40014 Jyväskylä, Finland; matti.o.haukka@jyu.fi

* Correspondence: ambarakat@ksu.edu.sa; Tel.: +966-11467-5901; Fax: +966-11467-5992

Received: 31 July 2020; Accepted: 8 August 2020; Published: 10 August 2020



Abstract: The 1,3-dipolar cycloaddition reaction is one of the most rapid, and efficient protocols to access, and construct highly divergent heterocycle chiral auxiliaries. Free catalyst synthesis of spirooxindole scaffold incorporating sulphone moiety via one pot–three component reaction of 6-chloro-isatin, L-proline, and the phenylvinylsulphone as dienophile is presented. The new regioisomer and diastereomer was isolated by precipitation without the tedious purification step, and then characterized via NMR and single crystal X-ray diffraction analysis. Using Hirshfeld analysis, the analysis of molecular packing was performed. It depended mainly on strong O . . . H and N . . . H interactions, and weak H . . . H, C . . . H, and Cl . . . H interactions as well. DFT calculations were used to optimize the experimental X-ray structure, which was found well matched with the calculated one. Reactivity descriptors based on the energies of the highest occupied (HOMO) and lowest unoccupied (LUMO) molecular orbitals were calculated. Additionally, the donor–acceptor interactions which stabilized the system via $\sigma\text{-}\sigma^*$, $\pi\text{-}\pi^*$, $n\text{-}\sigma^*$ and $n\text{-}\pi^*$ electron delocalization processes were also computed using NBO calculations. The net interaction energies are 49.96, 235.38, 179.66 and 107.06 kJ/mol, respectively. Additionally, the calculated NMR chemical shifts correlated well with the experimental data ($R^2=0.99$).

Keywords: spirooxindole; sulphone; 1,3-dipolar cycloaddition reaction; regioisomer; diastereomer; Hirshfeld analysis

1. Introduction

The design and discovery of new and applicable materials are of great interest in the scientific community. Specifically, asymmetric synthesis is a type of chemical synthesis that has been proven to offer requisite materials in enantioselective and diastereoselective forms. In modern chemistry particularly, enantioselective synthesis is important in the field of pharmaceuticals and agriculture chemistry in which the different forms of the enantiomers or diastereomers of the specific molecules have different efficacy due to unique and exploitable properties in optically pure forms [1].

Spirooxindole is a privileged structure and has been studied extensively by chemists and pharmacists. Spirooxindoles have exceptional structural topographies in 3D and are known to be

the best privileged chemotypes for sundry biological targets (Figure 1). This interesting scaffold has been found in diverse natural as well as synthetic compounds [2]. Examples of naturally occurring compounds proven to have preventative activity against human cancer are the spirotryprostatins A and B [3]. Indeed, spirooxindole alkaloids were proven to act as neuroprotective agents (such as anticonvulsant, antipyretic, and antihypertensive medicine). For example, rhynchophylline is an *N*-methyl-D-aspartate receptor antagonist [4]. Furthermore, mitraphylline has an *in vivo* controlling effect against the cytokines linked with most inflammation processes. Thus, mitraphylline can be employed as a template in anti-inflammatory therapy [5]. Welwitindolinone A isonitrile is a marine alkaloid incorporating the spirooxindole motif structure and has been shown to have anti-fungal efficacy [6].

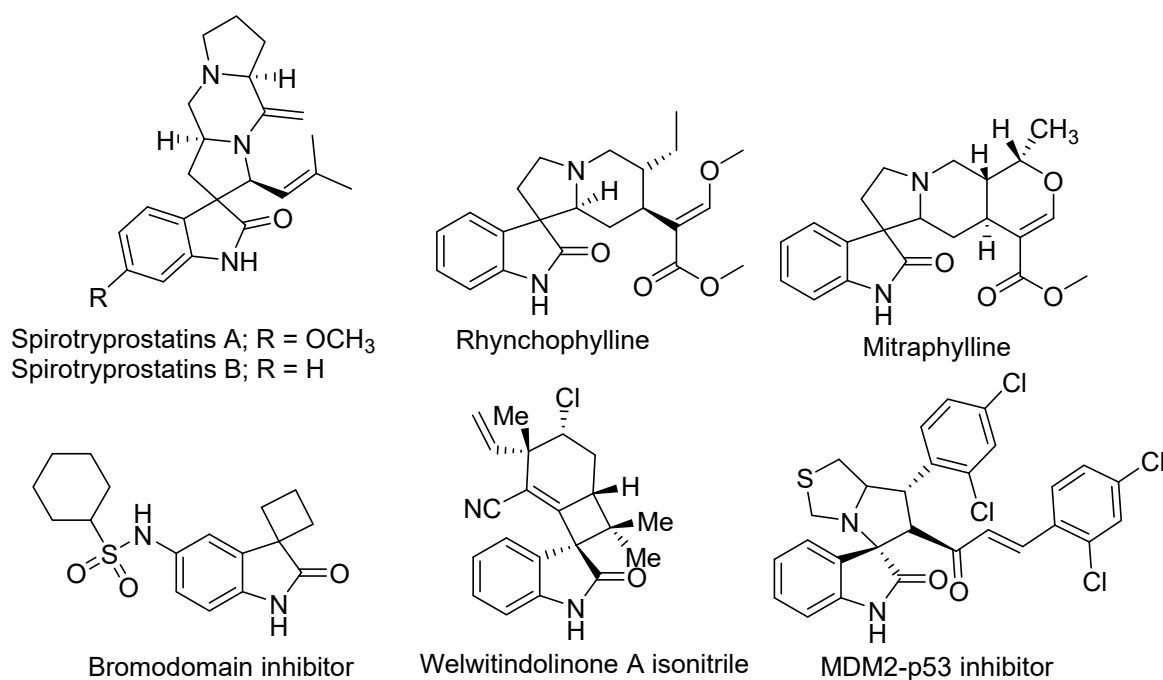


Figure 1. Biologically active compounds based on the spirooxindole scaffold.

On the other hand, many synthesized spirooxindole family members have been proven to have significant biological activities (e.g., anti-inflammatory, anticancer, analgesic, bromodomain inhibitor, antimicrobial, antimalarial, antioxidant, antiviral, antidiabetic, antiatherosclerotic, and insecticidal activities) and unique spatial architectures. Additionally, spirooxindole received the remarkable attention of many pharmacologists and chemists [6–23].

The most rapid and efficient method to construct highly complex heterocyclic chiral auxiliaries without a tedious purification process is the 1,3-dipolar cycloaddition reaction [24–26]. Thus, we employed this fascinating approach for the synthesis of a new spirooxindole having a sulphone moiety in enantioselective and diastereoselective fashion. Indeed, the conformational constrained rings in the synthesized compound were investigated and assigned.

2. Materials and Methods

The ¹H NMR and ¹³C-NMR spectra of **4** were recorded on a JEOL 400-MHz spectrometer (JEOL, Ltd, Tokyo, Japan) at ambient temperature. The solvent used was DMSO-*d*₆; the chemical shifts (δ) were given in ppm. Single-crystal X-ray data of compound **4** were collected on a Rigaku Oxford Diffraction Supernova diffractometer at 120 K. The crystallographic details are provided as supplementary material. Crystal Explorer 17.5 program was used for the Hirshfeld analysis [27].

2.1. Synthesis of the Spirooxindole-Based Phenylsulphone ((1'R,3R,7a'R)-6-Chloro-1'-(phenylsulfonyl)-1',2',5',6',7',7a'-hexahydrospiro[indoline-3,3'-pyrrolizin]-2-one **4**)

A mixture of phenylvinylsulphone (168 mg, 1.0 mmol), 6-chloro-isatin (181 mg, 1.0 mmol), and L-proline (115 mg, 1.0 mmol) in methanol (10 mL) was refluxed in an oil bath for appropriate time 8 h. After completion of the reaction as evident from TLC, the reaction was kept at room temperature overnight, and the solid crystalline product was filtered off without any further purification.

^1H NMR (400 MHz, DMSO- D_6) δ 10.45 (s, 1H), 7.94 (d, J = 7.8 Hz, 2H), 7.76 (t, J = 7.4 Hz, 1H), 7.66 (t, J = 7.6 Hz, 2H), 7.43 (d, J = 8.1 Hz, 1H), 7.04 (d, J = 7.8 Hz, 1H), 6.81 (s, 1H), 4.47 (dt, J = 11.3, 8.0 Hz, 1H), 4.00 (q, J = 7.9 Hz, 1H), 3.33 (d, J = 12.2 Hz, 1H), 2.78 (td, J = 9.1, 6.4 Hz, 1H), 2.56–2.45 (m, 2H), 2.37–2.22 (m, 1H), 2.08–1.83 (m, 2H), 1.71–1.56 (m, 1H); ^{13}C NMR (101 MHz, DMSO- d_6) δ 179.55, 144.93, 139.29, 135.14, 134.96, 130.44, 128.52, 127.64, 125.12, 122.17, 110.52, 104.52, 69.35, 68.96, 62.52, 53.28, 34.56, 32.64.

2.2. X-ray Structure Determinations

The crystal of **4** was immersed in cryo-oil, mounted in a loop, and measured at a temperature of 120 K. The X-ray diffraction data were collected on a Rigaku Oxford Diffraction Supernova diffractometer using Mo $K\alpha$ radiation. The CrysAlisPro [28] software package was used for cell refinement and data reduction. An analytical absorption correction (CrysAlisPro [28]) was applied to the intensities before structure solution. The structure was solved by intrinsic phasing (SHELX [29]) method. Structural refinement was carried out using SHELXL [29] software with SHELXLE [30] graphical user interface. The NH hydrogen atom was located from the difference Fourier map and refined isotropically. All other hydrogen atoms were positioned geometrically and constrained to ride on their parent atoms, with C–H = 0.95–1.00 Å and $U_{\text{iso}} = 1.2 U_{\text{eq}}$ (parent atom). The crystallographic details are summarized in Table 1.

2.3. Computational Methods

All DFT calculations were performed using the Gaussian 09 software package [31,32] utilizing the B3LYP/6-31G(d,p) method. Natural bond orbital analyses were performed using the NBO 3.1 program as implemented in the Gaussian 09W package [33]. The self-consistent reaction field (SCRFF) method [34,35] was used to model the solvent effects, including the polarizable continuum model (PCM), when calculating the optimized geometry in solution. Then, the NMR chemical shifts for the protons and carbons were computed using the GIAO method in the same solvent (DMSO) [36].

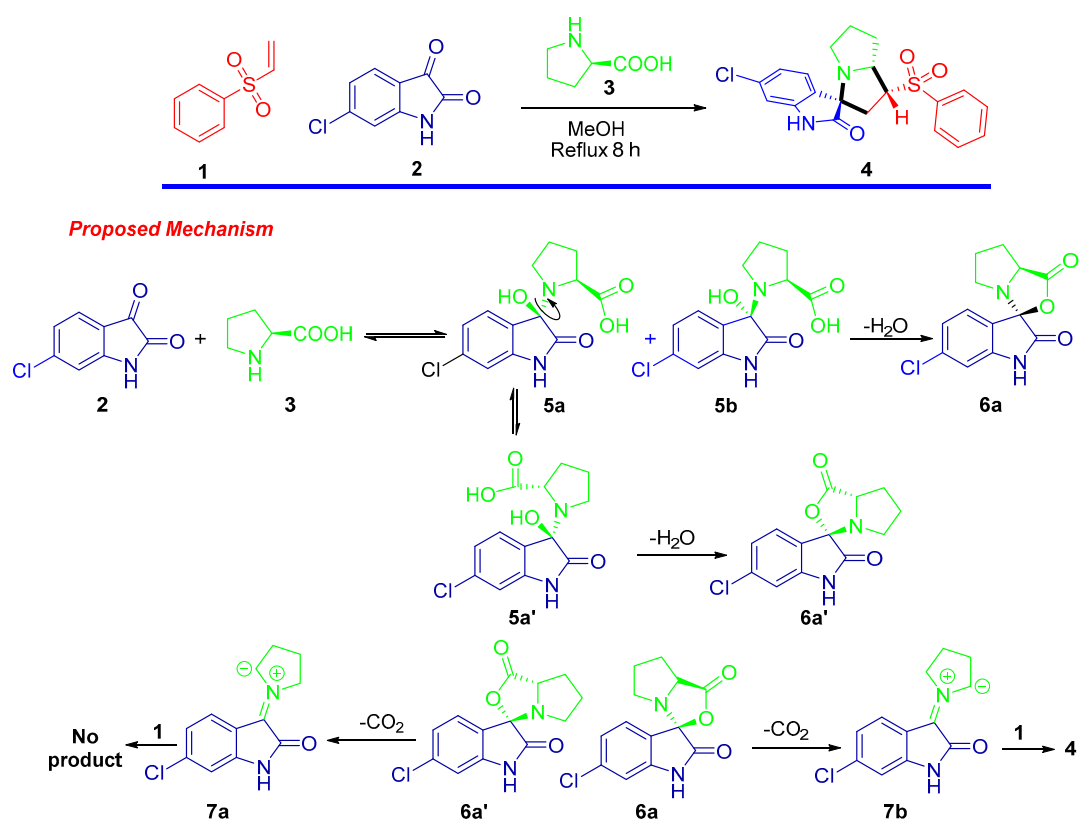
3. Results

3.1. Synthesis of the Spirooxindole-Based Phenylsulphone **4**

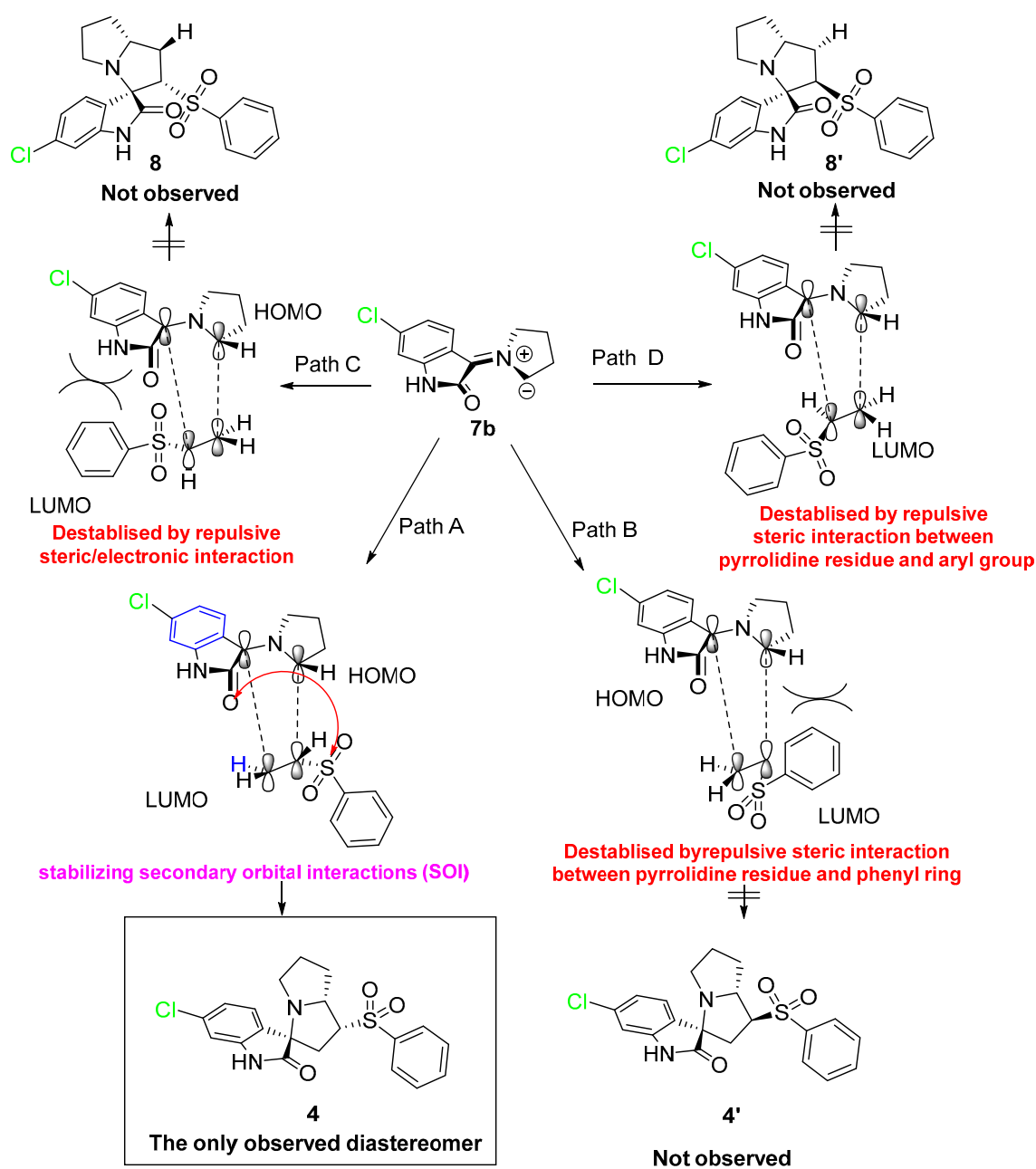
The design and construction of a new material with a significant application for the scientific community is a challenge. In this context we employed the one pot–multi component 1,3-dipolar cycloaddition approach for the synthesis of spirooxindole-based phenylsulphone as a new material [37]. The synthetic route is depicted in Scheme 1. The cycloadduct was obtained via reaction of phenylvinylsulphone as dienophile with the generated azomethine ylide by reaction of 6-chloro-isatin with the secondary amino acid (L-proline) under thermal condition. The target compound was afforded in a high chemical yield with regioselective and diastereoselective fashion. The chemical architecture was assigned based on a number of spectrophotometric tools including single crystal X-ray diffraction analysis plus ^1H NMR, and ^{13}C NMR spectral analysis. The result of ^1H NMR analysis exhibited the characteristic peaks of the assigned protons as follows: the secondary amine functionality peaks were shown as singlet at δ 10.45 ppm; the aromatic protons corresponding to the benzene and oxindole rings were located in the chemical shift region between δ 7.94 and 6.81 ppm; the aliphatic shielded protons belonging to the hexahydro-1H-pyrrolizine appeared in the upfield region with the range of δ 4.47–1.56 ppm. The ^{13}C -NMR spectra were consistent with the expected carbons of the chemical feature in the synthesized compound. The stereochemical and regio-specific outcomes of the

reaction were confirmed by HNMR and X-ray single diffraction analysis. Based on the experimental results and similar previous reports, a plausible mechanism for the regio- and diastereoselective spirooxindole-based phenylsulphone **4** presented in Scheme 1 might be proposed.

First, the generation of the stabilized azomethine ylide **6a** by a set of chemical reactions including condensation was followed by thermal decarboxylation reactions of the 5-chloroisatin with the L-proline. Subsequently, the generated azomethine ylide reacted with the dipolarophile **1** via the 1,3-dipolar cycloaddition reaction affording the desired cycloadduct in a completely regio- and stereoselective manner. The highly cycloadduct formation may be directed by the presence of stabilizing secondary orbital interactions between the 2-oxindoline and the sulphone function of the dipolarophile. This method/multicomponent reaction can be extendable for other starting materials/products.



Scheme 1. Cont.



Scheme 1. Synthesis of spirooxindole-based phenylsulphone **4**.

3.2. X-ray Structure of **4**

The structure of the new material **4** crystallized in the monoclinic crystal system and space group $I2/a$ with one molecule per asymmetric unit and $Z = 8$. The structure details and refinement parameters are listed in Table 1. The X-ray structure at 50% probability level along with atom numbering is given in Figure 2, while the bond distances and angles are listed in Table 2 and Table S1 (Supplementary data), respectively. The molecular structure of the new material **4** comprised one intramolecular C7–H7...O3 interaction with a donor–acceptor distance of 3.001(2) Å (Table 3). The C7–H7...O3 interaction is emphasized by the turquoise dotted line in Figure 3 (left part), while the red dotted line represents the intermolecular contacts.

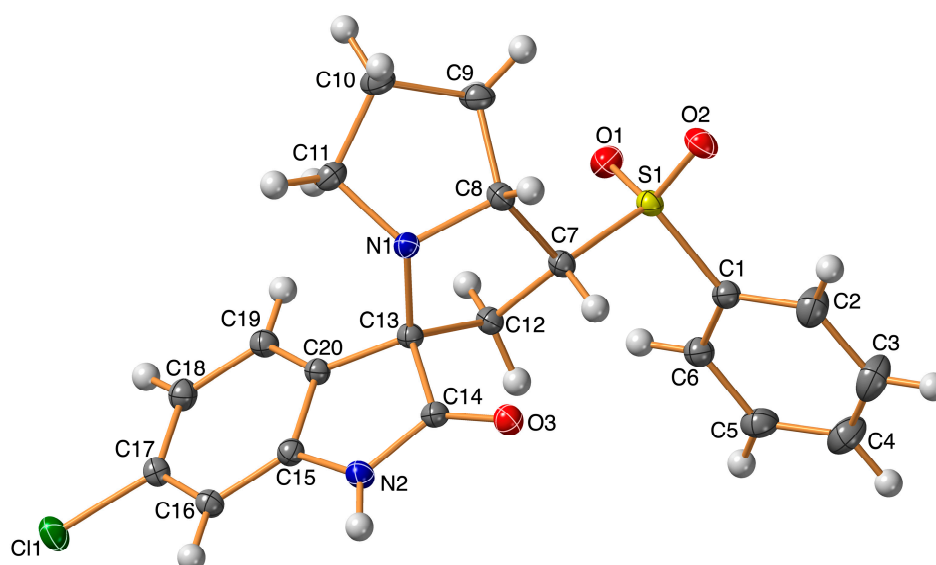


Figure 2. X-ray structure showing atom numbering and thermal ellipsoids at 50% probability level.

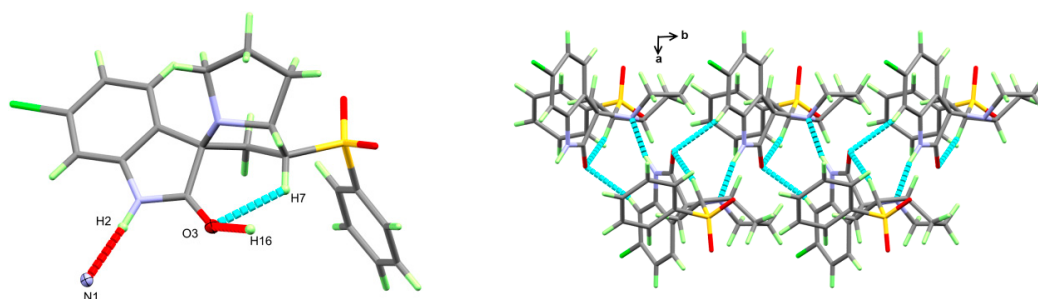


Figure 3. Intermolecular contacts (left) and packing (right) of molecular units in the new material 4.

Table 1. Crystal data.

4	
empirical formula	C ₂₀ H ₁₉ ClN ₂ O ₃ S
fw	402.88
temp (K)	120(2)
λ (Å)	0.71073
cryst syst	Monoclinic
space group	I ₂ /a
<i>a</i> (Å)	22.2636(6)
<i>b</i> (Å)	7.70240(10)
<i>c</i> (Å)	24.3057(6)
β (deg)	116.521(3)
<i>V</i> (Å ³)	3729.42(17) Å ³
<i>Z</i>	8
ρ_{calc} (Mg/m ³)	1.435 Mg/m ³
μ (Mo K α) (mm ⁻¹)	0.341 mm ⁻¹
No. reflns.	10411
Unique reflns.	5073
GOOF (F ²)	1.037
<i>R</i> _{int}	0.0147
<i>R</i> ₁ ^a (<i>I</i> ≥ 2 σ)	0.0333
<i>wR</i> ₂ ^b (<i>I</i> ≥ 2 σ)	0.0831
CCDC	2020273

^a $R_1 = \Sigma||F_o| - |F_c||/\Sigma|F_o|$. ^b $wR_2 = [\Sigma[w(F_o^2 - F_c^2)^2]/\Sigma[w(F_o^2)^2]]^{1/2}$.

Table 2. Selected bond lengths (Å) for the new material **4**.

Cl(1)–C(17)	1.7395(13)
S(1)–O(2)	1.4402(10)
S(1)–O(1)	1.4450(10)
S(1)–C(1)	1.7652(13)
S(1)–C(7)	1.7873(12)
O(3)–C(14)	1.2208(15)
N(1)–C(11)	1.4912(16)
N(1)–C(13)	1.4986(15)
N(1)–C(8)	1.5055(15)
N(2)–C(14)	1.3606(16)
N(2)–C(15)	1.4052(16)
N(2)–H(2)	0.913(18)

Table 3. Hydrogen-bond geometry (Å, °).

<i>D</i> –H... <i>A</i>	<i>D</i> –H	H... <i>A</i>	<i>D</i> ... <i>A</i>	<i>D</i> –H... <i>A</i>
N2–H2...N1 ^{#1}	0.913(2)	1.963(2)	2.862(1)	168.0(2)
C7–H7...O3	1.00	2.37	3.001(2)	120.5
C16–H16...O3 ^{#1}	0.95	2.41	3.106(2)	129.0

Symmetry codes: #1; $-x + 1, y - 1/2, -z + 1/2$.

The molecular packing of the new material **4** was controlled mainly by the strong N2–H2...N1 hydrogen bond and weak C16–H16...O3 interaction listed in Table 2 and shown as red dotted lines in Figure 3 (left part). The donor–acceptor distances for these interactions were 2.862(1) and 3.106(2) Å, respectively. In addition, the right part of this figure shows the packing of the different molecular units along the *ab*-direction.

3.3. Hirshfeld Analysis of Molecular Packing

The different maps resulting from Hirshfeld calculations are presented in Figure 4. With the aid of fingerprint plots, quantitative analysis of the different contacts was performed, and the percentage contribution of each contact is shown in Figure 5. The molecules were packed in the crystal via strong Cl...H (10.2%), O...H (21.9%), and N...H (3.7%) contacts. The shortest Cl...H and N...H interactions were Cl1...H11B (2.857 Å) and N1...H2 (1.870 Å), respectively. There were many O...H contacts, with interaction distances ranging from 2.330 Å to 2.575 Å. The most important O...H interactions were O2...H2A (2.565 Å), O2...H5 (2.575 Å), O3...H16 (2.330 Å), O3...H4 (2.538 Å), and O1...H19 (2.382 Å). The relevance of these interactions is indicated from the decomposed d_{norm} maps shown in Figure 6. The Cl...H contacts appeared as white regions, indicating weak interactions, while the more important N...H and O...H contacts appeared as red spots in the d_{norm} maps. In addition to these contacts, the packing was controlled by some weak H...H (40.7%), C...H (17.9%), and C...C (2.1%) interactions.

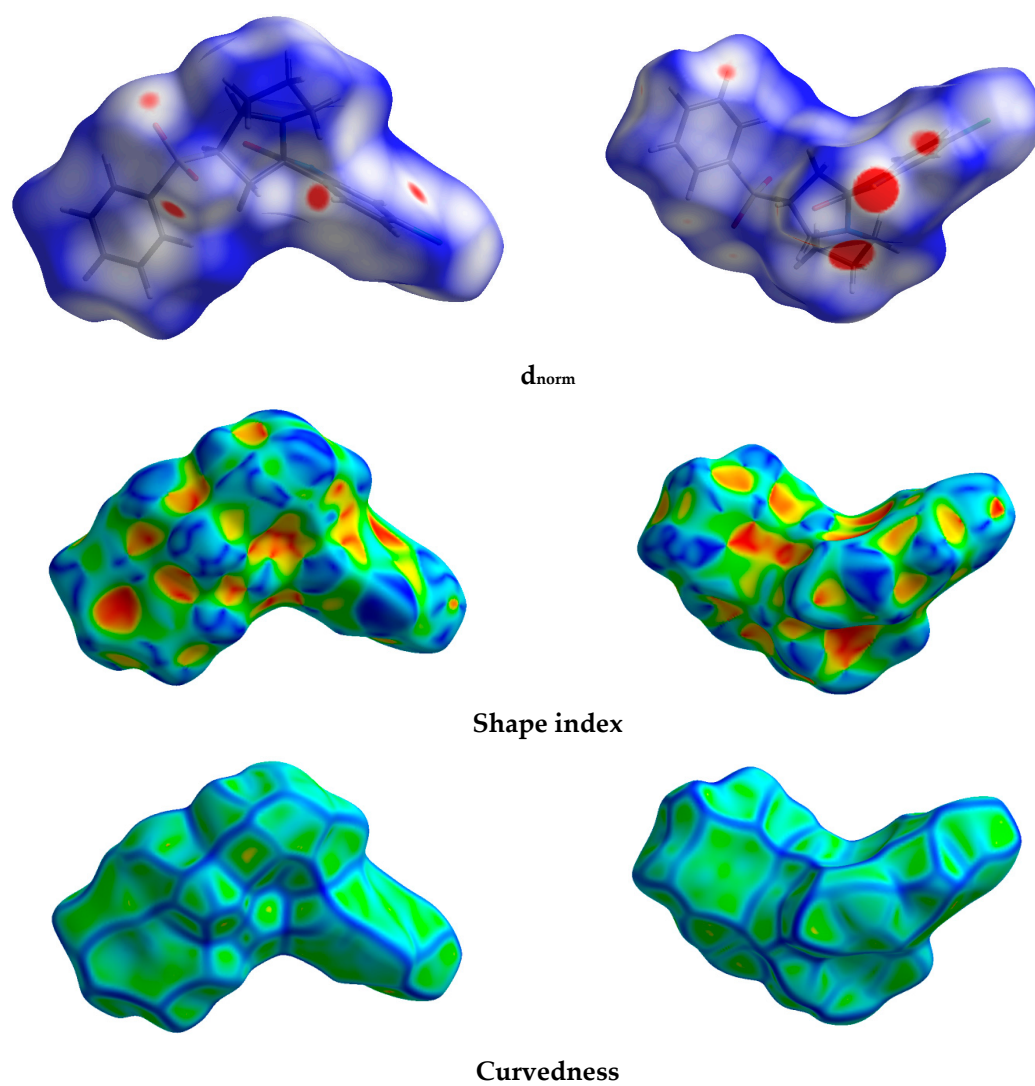


Figure 4. Hirshfeld surfaces of the new material 4.

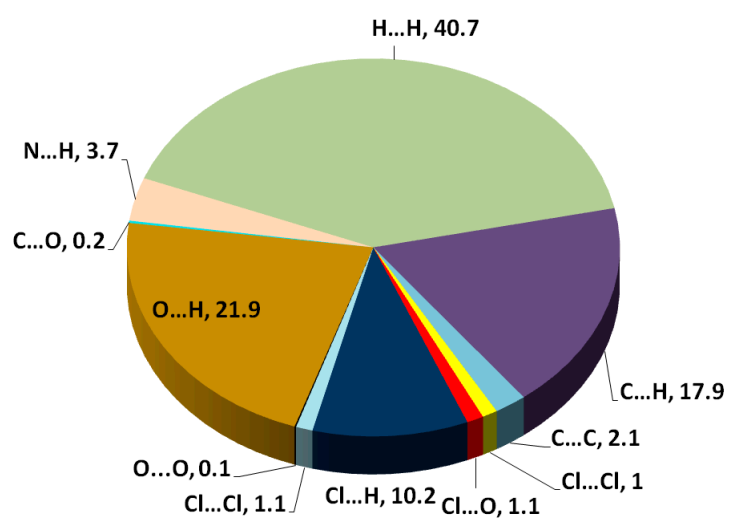


Figure 5. Pie chart for the intermolecular interactions and their percentage contributions.

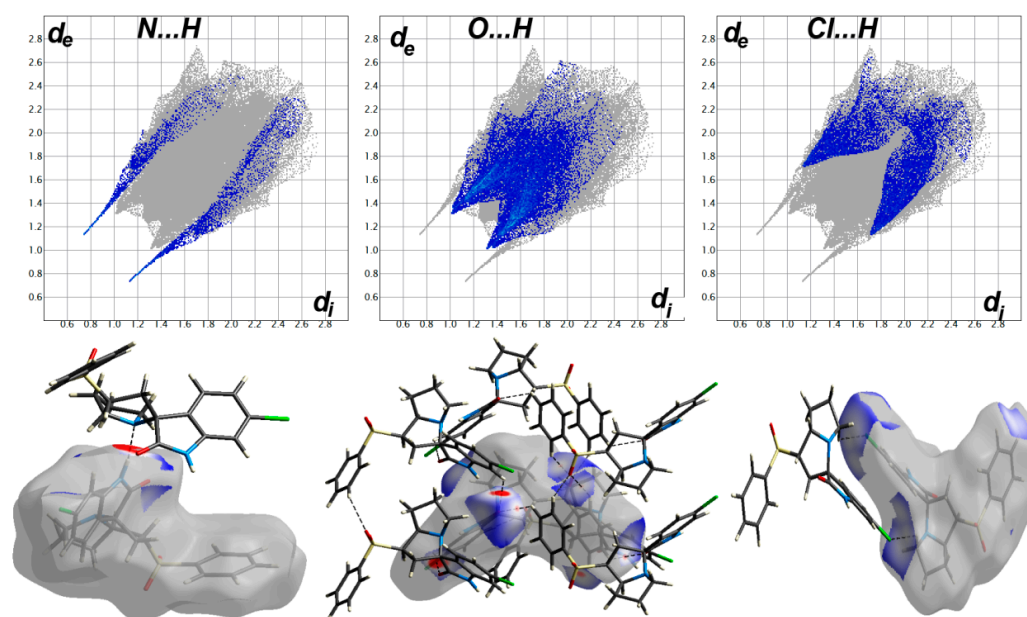


Figure 6. Fingerprint plots (**upper**) and d_{norm} surfaces (**lower**) of the N...H, O...H and Cl...H contacts.

3.4. DFT Studies

The optimized geometry of the new material **4** is presented in Figure 7 along with structure matching between the computed molecular geometry with the experimental one. With the high correlation coefficients ($R^2 = 0.98$) between the calculated and experimental geometric parameters (Figure 8), the calculated structure agreed very well with the experimental one. A list of the calculated and experimental geometric parameters is given in Table S2 (Supplementary materials).

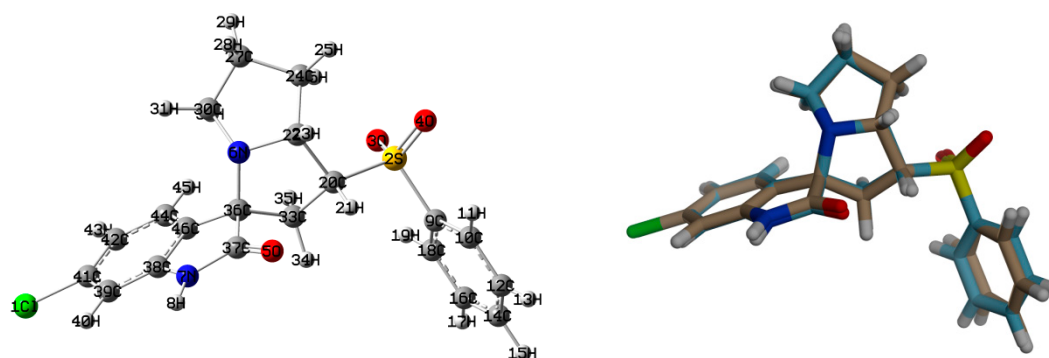


Figure 7. The optimized geometry (**left**) and overlay of the optimized with experimental structures, (**right**) for the new material **4**.

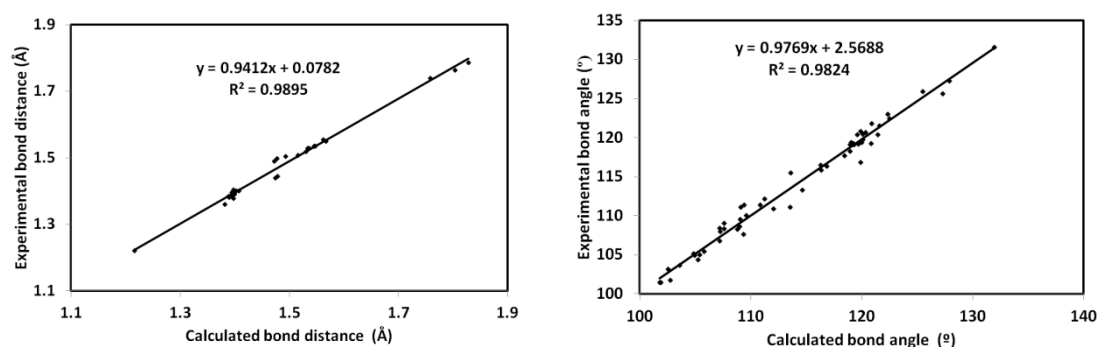


Figure 8. The straight line correlations between the calculated and experimental geometric parameters.

The partial atomic charges on the basis of natural population analysis are listed in Table 4. Interestingly, the sulphur atom of the SO₂ moiety had the highest positive charge (2.216 e). In contrast, the corresponding oxygen atoms were the most electronegative. Generally, all hydrogen sites as well as carbon atoms attached to N or O atoms had positive partial charges. The electron density distribution over molecular electrostatic potential (MESP) shown in Figure 9 confirmed the high electron density related to all O-sites, while the opposite was true for the NH proton. These sites represented the most favored sites for hydrogen bonding interactions as hydrogen bond acceptor and hydrogen bond donor, respectively. Additionally, the compound was polar (3.965 Debye) and the dipole moment vector was in the direction of the sulphone group.

Table 4. Natural atomic charges of the new material 4 ^a.

Atom	Charge	Atom	Charge	Atom	Charge
C11	0.0020	H 17	0.2481	H 32	0.2020
S2	2.2162	C 18	-0.2195	C 33	-0.4776
O3	-0.9644	H 19	0.2682	H 34	0.2623
O4	-0.9524	C 20	-0.5068	H 35	0.2630
O5	-0.5983	H 21	0.2960	C 36	0.0524
N6	-0.5097	C 22	-0.0639	C 37	0.7268
N7	-0.6325	H 23	0.2621	C 38	0.1914
H8	0.4439	C 24	-0.4907	C 39	-0.2913
C9	-0.3220	H 25	0.2645	H 40	0.2604
C 10	-0.2168	H 26	0.2526	C 41	-0.0222
H 11	0.2671	C 27	-0.4692	C 42	-0.2735
C 12	-0.2300	H 28	0.2403	H 43	0.2605
H 13	0.2492	H 29	0.2501	C 44	-0.1958
C 14	-0.2167	C 30	-0.2589	H 45	0.2517
H 15	0.2464	H 31	0.2428	C 46	-0.0759
C 16	-0.2318				

^a Atom numbering refer to Figure 7.

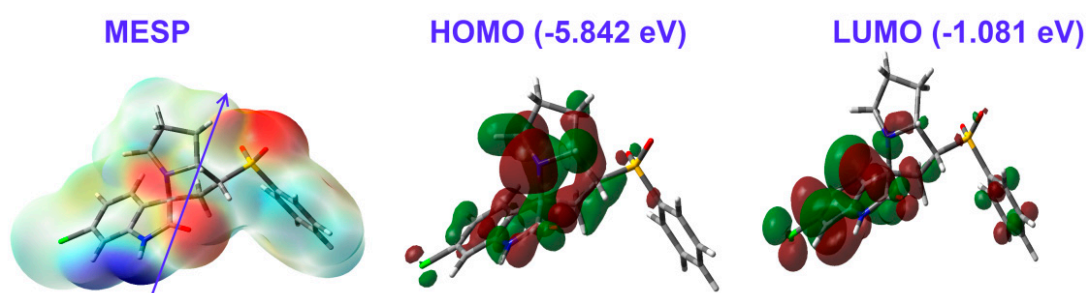


Figure 9. The MESP, highest occupied (HOMO), and lowest unoccupied (LUMO) molecular orbitals of the new material 4.

In addition, the HOMO and LUMO frontier molecular orbitals are important for the molecule reactivity [38–44]. Their energies were calculated to be -5.842 and -1.081 eV, respectively. Hence, the calculated ionization potential (I) and electron affinity (A) were 5.842 and 1.081 eV, respectively. Additionally, the hardness, electrophilicity index, and chemical potential were 4.761 , 1.258 , and -3.461 eV, respectively. Since, the HOMO was located over the two fused ring systems, while the LUMO was

localized over the fused aromatic π -system, the HOMO \rightarrow LUMO excitation represented mixed $n\rightarrow\pi^*$ and $\pi\rightarrow\pi^*$ transitions with an energy of 4.761 eV.

3.5. NBO Analysis

The stabilization energies ($E^{(2)}$) resulting from the electron delocalizations among natural orbitals [45,46] are listed in Table 5. The $\sigma\rightarrow\sigma^*$ electron delocalization processes were the weakest where the maximum $E^{(2)}$ value was 5.62 eV ($\sigma(\text{C39-C41})\rightarrow\sigma^*(\text{N7-C38})$) and the net $\sigma\rightarrow\sigma^*$ interaction energy was 49.96 kcal/mol. On other hand, the maximum $E^{(2)}$ values for the $n\rightarrow\sigma^*$, $\pi\rightarrow\pi^*$, and $n\rightarrow\pi^*$ electron delocalizations were 23.29, 23.62, and 55.29 kcal/mol for $n(\text{O4})\rightarrow\sigma^*(\text{S2-O3})$, $\pi(\text{C14-C16})\rightarrow\pi^*(\text{C9-C18})$, and $n(\text{N7})\rightarrow\pi^*(\text{O5-C37})$ interactions, respectively. The net stabilization energy was higher for $\pi\rightarrow\pi^*$ (235.38 kcal/mol) than for the $n\rightarrow\sigma^*$ (179.66 kcal/mol) and $n\rightarrow\pi^*$ (107.06 kcal/mol) interactions.

Table 5. The $E^{(2)}$ (kcal/mol) values for the charge transfer interactions in the new material 4 ^a.

Donor NBO	Acceptor NBO	$E^{(2)}$	Donor NBO	Acceptor NBO	$E^{(2)}$
<u>$\sigma\rightarrow\sigma^*$</u>			<u>$\pi\rightarrow\pi^*$</u>		
BD (1) C9-C10	BD*(1) C9-C18	4.29	BD (2) C9-C18	BD*(2) C10-C12	20.61
BD (1) C9-C18	BD*(1) C9-C10	4.29	BD (2) C9-C18	BD*(2) C14-C16	17.09
BD (1) C36-C37	BD*(1) C44-C46	4.29	BD (2) C10-C12	BD*(2) C9-C18	19.55
BD (1) C38-C39	BD*(1) C11-C41	4.31	BD (2) C10-C12	BD*(2) C14-C16	21.02
BD (1) C38-C39	BD*(1) C38-C46	4.68	BD (2) C14-C16	BD*(2) C9-C18	23.62
BD (1) C38-C46	BD*(1) C38-C39	4.15	BD (2) C14-C16	BD*(2) C10-C12	18.94
BD (1) C39-C41	BD*(1) N7-C38	5.62	BD (2) C38-C39	BD*(2) C41-C42	22.22
BD (1) C42-C44	BD*(1) C36-C46	5.11	BD (2) C38-C39	BD*(2) C44-C46	16.53
BD (1) C42-C44	BD*(1) C11-C41	4.71	BD (2) C41-C42	BD*(2) C38-C39	15.95
BD (1) C44-C46	BD*(1) C38-C46	4.13	BD (2) C41-C42	BD*(2) C44-C46	19.37
BD (2) C44-C46	BD*(1) N6-C36	4.38	BD (2) C44-C46	BD*(2) C38-C39	22.64
			BD (2) C44-C46	BD*(2) C41-C42	18.29
<u>$n\rightarrow\sigma^*$</u>			<u>$n\rightarrow\pi^*$</u>		
LP (2) O3	BD*(1) S2-C9	13.08	LP (1) N7	BD*(2) O5-C37	55.29
LP (2) O3	BD*(1) S2-C20	15.29	LP (1) N7	BD*(2) C38-C39	39.34
LP (3) O3	BD*(1) S2-O4	22.48	LP (3) C11	BD*(2) C41-C42	12.43
LP (3) O3	BD*(1) S2-C9	6.45			
LP (3) O3	BD*(1) S2-C20	4.24			
LP (2) O4	BD*(1) S2-C9	13.03			
LP (2) O4	BD*(1) S2-C20	15.61			
LP (3) O4	BD*(1) S2-O3	23.29			
LP (3) O4	BD*(1) S2-C9	6.98			
LP (2) O5	BD*(1) N7-C37	27.9			
LP (2) O5	BD*(1) C36-C37	22.37			
LP (1) N6	BD*(1) C33-C36	4.96			
LP (1) N6	BD*(1) C36-C37	3.98			

^a Atom numbering refer to Figure 7.

3.6. NMR Spectra

The chemical shifts (C.S) of ^1H and ^{13}C were computed and the results are listed in Table S3 (Supplementary materials) in comparison with the experimental data. It is clear from Figure 10 that there was a good relation between the experimental and calculated C.S values. The correlation coefficients were very close to 1.

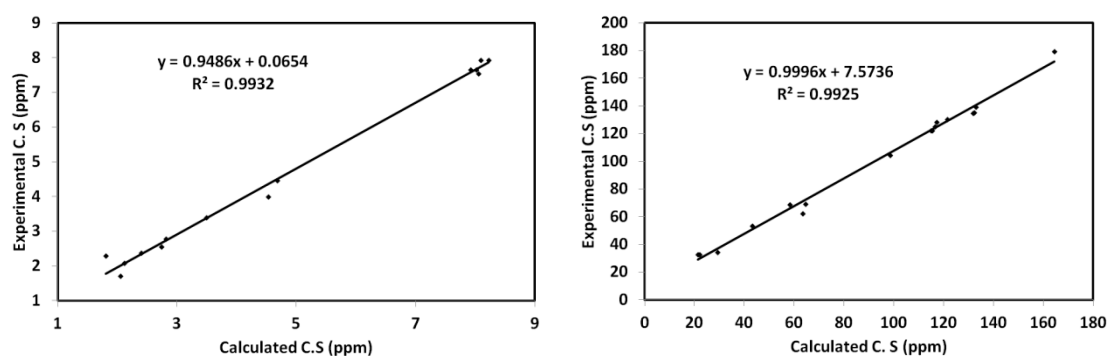


Figure 10. Correlation graphs between the calculated and experimental ^1H and ^{13}C NMR chemical shifts.

4. Conclusions

In the sustained search for new compounds, we report herein the synthesis of a novel spirooxindole-based sulfone function by one pot–three component 1,3-dipolar cycloaddition of stabilized azomethine ylides, generated in situ by condensation of 6-chloro-isatin and L-proline with phenylvinylsulphone. The highlight of this protocol is the efficient high-yield construction of a novel spirooxindole analogue, including three contiguous stereocenters, along with excellent regio- and diastereoselectivities. The stereochemistry of the newly synthesized compound is confirmed by NMR and corroborated by the X-ray diffraction study performed on **4**. Using Hirshfeld analysis, the O...H (21.9%), H...H (40.7%), and C...H (17.9%) contributed heavily to the intermolecular interactions included in the molecular packing, which support the crystal stability. Based on the d_{norm} map, the N...H and O...H contacts are the most significant interactions. The calculated structure matched well with the experimental one. The net $\sigma\text{-}\sigma^*$, $\pi\text{-}\pi^*$, $n\text{-}\sigma^*$, and $n\text{-}\pi^*$ interactions stabilized the system by 49.96, 235.38, 179.66, and 107.06 kcal/mol, respectively, using NBO calculations.

Supplementary Materials: The following are available online at <http://www.mdpi.com/2073-8994/12/8/1337/s1>. Figure S1 & S2: NMR spectrum of the synthesized compound, Table S1: Bond angles; Table S2: calculated geometric parameters of the studied compound; Table S3: calculated and experimental chemical shifts (ppm) of the studied compound.

Author Contributions: Conceptualization, A.B.; data curation, S.M.S. and M.H.; formal analysis, M.H., M.A., and M.R.S.; funding acquisition, A.B.; investigation, M.S.I.; methodology, M.S.I. and M.A.; software, S.M.S. and M.H.; validation, A.M.A.-M.; visualization, A.M.A.-M.; writing—original draft, A.B. and S.M.S.; writing—review and editing, A.B. and S.M.S. All authors have read and agreed to the published version of the manuscript.

Funding: The authors would like to extend their sincere appreciation to the Researchers Supporting Project, Number (RSP-2020/64), King Saud University, Riyadh, Saudi Arabia.

Acknowledgments: The authors would like to extend their sincere appreciation to the Researchers Supporting Project, Number (RSP-2020/64), King Saud University, Riyadh, Saudi Arabia.

Conflicts of Interest: The authors declare no conflict of interest.

References

- Ojima, I. *Catalytic Asymmetric Synthesis*; John Wiley & Sons: Hoboken, NJ, USA, 2004.
- Zhou, L.M.; Qu, R.Y.; Yang, G.F. An overview of spirooxindole as a promising scaffold for novel drug discovery. *Expert Opin. Drug Discov.* **2020**, *15*, 603–625. [[CrossRef](#)] [[PubMed](#)]
- Ding, K.; Lu, Y.; Nikolovska-Coleska, Z.; Qiu, S.; Ding, Y.; Gao, W.; Stuckey, J.; Krajewski, K.; Roller, P.P.; Tomita, Y.; et al. Structure-based design of potent non-peptide MDM2 inhibitors. *J. Am. Chem. Soc.* **2005**, *127*, 10130–10131. [[CrossRef](#)] [[PubMed](#)]
- Kang, T.H.; Murakami, Y.; Matsumoto, K.; Takayama, H.; Kitajima, M.; Aimi, N.; Watanabe, H. Rhynchophylline and isorhynchophylline inhibit NMDA receptors expressed in *Xenopus* oocytes. *Eur. J. Pharmacol.* **2002**, *455*, 27–34. [[CrossRef](#)]

5. Rojas-Duran, R.; González-Aspajo, G.; Ruiz-Martel, C.; Bourdy, G.; Doroteo-Ortega, V.H.; Alban-Castillo, J.; Robert, G.; Auberger, P.; Deharo, E. Anti-inflammatory activity of Mitrephylline isolated from *Uncaria tomentosa* bark. *J. Ethnopharmacol.* **2012**, *143*, 801–804. [[CrossRef](#)]
6. Stratmann, K.; Moore, R.E.; Patterson, G.M.L.; Bonjouklian, R.; Deeter, J.B.; Shaffer, S.; Smitka, T.A.; Smith, C.D. Welwitindolinones, unusual alkaloids from the blue-green algae *Hapalosiphon welwitschii* and *Westiella intricata*. Relationship to fischerindoles and hapalinodoles. *J. Am. Chem. Soc.* **1994**, *116*, 9935–9942. [[CrossRef](#)]
7. Santos, M.M. Recent advances in the synthesis of biologically active spirooxindoles. *Tetrahedron* **2014**, *52*, 9735–9757. [[CrossRef](#)]
8. Pavlovska, T.L.; Redkin, R.G.; Lipson, V.V.; Atamanuk, D.V. Molecular diversity of spirooxindoles. Synthesis and biological activity. *Mol. Divers.* **2016**, *20*, 299–344. [[CrossRef](#)]
9. Arun, Y.; Bhaskar, G.; Balachandran, C.; Ignacimuthu, S.; Perumal, P. Facile one-pot synthesis of novel dispirooxindole-pyrrolidine derivatives and their antimicrobial and anticancer activity against a549 human lung adenocarcinoma cancer cell line. *Bioorg. Med. Chem. Lett.* **2013**, *23*, 1839–1845. [[CrossRef](#)]
10. Girgis, A.S. Regioselective synthesis of dispiro [1*H*-indene-2,3'-pyrrolidine-2', 3''-[3*H*]indole]-1,2''(1''h)-diones of potential anti-tumor properties. *Eur. J. Med. Chem.* **2009**, *44*, 91–100. [[CrossRef](#)]
11. Islam, M.S.; Park, S.; Song, C.; Kadi, A.A.; Kwon, Y.; Rahman, A.M. Fluorescein hydrazones: A series of novel non-intercalative topoisomerase II α catalytic inhibitors induce G1 arrest and apoptosis in breast and colon cancer cells. *Eur. J. Med. Chem.* **2017**, *125*, 49–67. [[CrossRef](#)] [[PubMed](#)]
12. Ali, M.A.; Ismail, R.; Choon, T.S.; Yoon, Y.K.; Wei, A.C.; Pandian, S.; Kumar, R.S.; Osman, H.; Manogaran, E. Substituted spiro [2.3'] oxindolespiro [3.2'']-5, 6-dimethoxy-indane-1''-one-pyrrolidine analogue as inhibitors of acetylcholinesterase. *Bioorg. Med. Chem. Lett.* **2010**, *20*, 7064–7066. [[CrossRef](#)]
13. Sharma, P.; Kumar, A.; Sahu, V.; Upadhyay, S.; Singh, J. Synthesis of bioactive spiro-2-[3'-(2'-phenyl)-3*h*-indolyl]-1-aryl-3-phenylaziridines and SAR studies on their antimicrobial behavior. *Med. Chem. Res.* **2009**, *18*, 383–395. [[CrossRef](#)]
14. Uchida, R.; Imasato, R.; Shiomi, K.; Tomoda, H.; Ōmura, S. Yaequinolones j1 and j2, novel insecticidal antibiotics from penicillium sp. Fki-2140. *Org. Lett.* **2005**, *7*, 5701–5704. [[CrossRef](#)] [[PubMed](#)]
15. Barakat, A.; Islam, M.S.; Ghawas, H.M.; Al-Majid, A.M.; El-Senduny, F.F.; Badria, F.A.; Elshaier, Y.A.; Ghabbour, H.A. Design and synthesis of new substituted spirooxindoles as potential inhibitors of the MDM2–p53 interaction. *Bioorg. Chem.* **2019**, *86*, 598–608. [[CrossRef](#)] [[PubMed](#)]
16. Altowyan, M.S.; Barakat, A.; Al-Majid, A.M.; Al-Ghulikah, H.A. Spiroindolone analogues bearing benzofuran moiety as a selective cyclooxygenase COX-1 with TNF- α and IL-6 inhibitors. *Saudi J. Biol. Sci.* **2020**, *27*, 1208–1216. [[CrossRef](#)] [[PubMed](#)]
17. Altowyan, M.S.; Barakat, A.; Al-Majid, A.M.; Al-Ghulikah, H. Spiroindolone analogues as potential hypoglycemic with dual inhibitory activity on α -amylase and α -glucosidase. *Molecules* **2019**, *24*, 2342. [[CrossRef](#)] [[PubMed](#)]
18. Islam, M.S.; Ghawas, H.M.; El-Senduny, F.F.; Al-Majid, A.M.; Elshaier, Y.A.; Badria, F.A.; Barakat, A. Synthesis of new thiazolo-pyrrolidine-(spirooxindole) tethered to 3-acylindole as anticancer agents. *Bioorg. Chem.* **2019**, *82*, 423–430. [[CrossRef](#)]
19. Barakat, A.; Islam, M.S.; Al-Majid, A.M.; Ghawas, H.M.; El-Senduny, F.F.; Badria, F.A.; Elshaier, Y.A.M. Ghabbour, Substituted spirooxindole derivatives as potent anticancer agents through inhibition of phosphodiesterase 1. *RSC Adv.* **2018**, *8*, 14335. [[CrossRef](#)]
20. Lotfy, G.; El Sayed, H.; Said, M.M.; Aziz, Y.M.A.; Al-Dhfyhan, A.; Al-Majid, A.M.; Barakat, A. Regio- and stereoselective synthesis of novel spiro-oxindole via 1,3-dipolar cycloaddition reaction. Anti-cancer and molecular docking studies. *J. Photochem. Photobiol. B* **2018**, *180*, 98–108. [[CrossRef](#)]
21. Barakat, A.; Soliman, S.M.; Al-majid, A.M.; Ali, M.; Islam, M.S.; Elshaier, Y.A.M.M.; Ghabbour, H.A. Regioselective synthesis of novel spiro-oxindole constructed with pyrrolidine/thioxothiazolidin-4-one derivatives: X-ray crystal structures, Hirshfeld surface analysis, DFT, docking and antimicrobial studies. *J. Mol. Struct.* **2018**, *1152*, 101–114. [[CrossRef](#)]
22. Lotfy, G.; Said, M.M.; El Sayed, H.; El Sayed, H.; Al-Dhfyhan, A.; Aziz, Y.M.A.; Barakat, A. Synthesis of new spirooxindole-pyrrolothiazoles derivatives: Anti-cancer activity and molecular docking. *Bioorg. Med. Chem.* **2017**, *25*, 1514–1523. [[CrossRef](#)] [[PubMed](#)]

23. Barakat, A.; Islam, M.S.; Al Majid, A.M.; Ghawas, H.M.; El-Senduny, F.F.; Badria, F.A.; M.Elshaier, Y.A.M.; Ghabbour, H.A. Substituted Spirooxindoles. U.S. Patent Application No. 9822128B1, 21 November 2017.
24. Rios, R. Enantioselective methodologies for the synthesis of spiro compounds. *Chem. Soc. Rev.* **2012**, *41*, 1060–1074. [[CrossRef](#)] [[PubMed](#)]
25. Hong, L.; Wang, R. Recent advances in asymmetric organocatalytic construction of 3, 3'-spirocyclic oxindoles. *Adv. Synth. Catal.* **2013**, *355*, 1023–1052. [[CrossRef](#)]
26. Jiang, X.; Sun, Y.; Yao, J.; Cao, Y.; Kai, M.; He, N.; Zhang, X.; Wang, Y.; Wang, R. Core Scaffold-Inspired Concise Synthesis of Chiral Spirooxindole-Pyranopyrimidines with Broad-Spectrum Anticancer Potency. *Adv. Synth. Catal.* **2012**, *354*, 917–925. [[CrossRef](#)]
27. Turner, M.J.; McKinnon, J.J.; Wolff, S.K.; Grimwood, D.J.; Spackman, P.R.; Jayatilaka, D.; Spackman, M.A. Crystal Explorer17 (2017) University of Western Australia. Available online: <http://hirshfeldsurface.net> (accessed on 12 June 2017).
28. Rikagu Oxford Diffraction. *CrysAlisPro*; Agilent Technologies Inc.: Yarnton, Oxfordshire, UK, 2018.
29. Sheldrick, G.M. SHELXT-Integrated space-group and crystal-structure determination. *Acta Cryst.* **2015**, *C71*, 3–8. [[CrossRef](#)] [[PubMed](#)]
30. Hübschle, C.B.; Sheldrick, G.M.; Dittrich, B. ShelXle: A Qt graphical user interface for SHELXL. *J. Appl. Cryst.* **2011**, *44*, 1281–1284. [[CrossRef](#)]
31. Frisch, M.J.; Trucks, G.W.; Schlegel, H.B.; Scuseria, G.E.; Robb, M.A.; Cheeseman, J.R.; Scalmani, G.; Barone, V.; Mennucci, B.; Petersson, G.A.; et al. *GAUSSIAN 09, Revision A02*; Gaussian Inc.: Wallingford, CT, USA, 2009.
32. Dennington, R., II; Keith, T.; Millam, J. (Eds.) *GaussView, Version 4.1*; Semichem Inc.: Shawnee Mission, KS, USA, 2007.
33. Reed, A.E.; Curtiss, L.A.; Weinhold, F. Intermolecular interactions from a natural bond orbital, donor-acceptor viewpoint. *Chem. Rev.* **1988**, *88*, 899–926. [[CrossRef](#)]
34. Marten, B.; Kim, K.; Cortis, C.; Friesner, R.A.; Murphy, R.B.; Ringnalda, M.N.; Sitkoff, D.; Honig, B. New Model for Calculation of Solvation Free Energies: Correction of Self-Consistent Reaction Field Continuum Dielectric Theory for Short-Range Hydrogen-Bonding Effects. *J. Phys. Chem.* **1996**, *100*, 11775–11788. [[CrossRef](#)]
35. Tannor, D.J.; Marten, B.; Murphy, R.; Friesner, R.A.; Sitkoff, D.; Nicholls, A.; Ringnalda, M.; Goddard, W.A.; Honig, B. Accurate first principles calculation of molecular charge distributions and solvation energies from ab initio quantum mechanics and continuum dielectric theory. *J. Am. Chem. Soc.* **1994**, *116*, 11875–11882. [[CrossRef](#)]
36. Cheeseman, J.R.; Trucks, G.W.; Keith, T.A.; Frisch, M.J. A Comparison of Models for Calculating Nuclear Magnetic Resonance Shielding Tensors. *J. Chem. Phys.* **1996**, *104*, 5497–5509. [[CrossRef](#)]
37. Al-Qubati, M.; Ghabbour, H.A.; Soliman, S.M.; Al-Majid, A.M.; Barakat, A.; Sultan, M.A. Synthesis of *N*-(Anthracen-9-ylmethyl)-*N*-methyl-2-(phenylsulfonyl)ethanamine via Microwave Green Synthesis Method: X-ray Characterization, DFT and Hirshfeld Analysis. *Crystals* **2020**, *10*, 643. [[CrossRef](#)]
38. Foresman, J.B.; Frisch, E. *Exploring Chemistry with Electronic Structure Methods*, 2nd ed.; Gaussian: Pittsburgh, PA, USA, 1996.
39. Chang, R. *Chemistry*, 7th ed.; McGraw-Hill: New York, NY, USA, 2001.
40. Kosar, B.; Albayrak, C. Spectroscopic investigations and quantum chemical computational study of (E)-4-methoxy-2-[(p-tolylimino) methyl] phenol. *Spectrochim. Acta* **2011**, *78*, 160–167. [[CrossRef](#)] [[PubMed](#)]
41. Koopmans, T.A. Ordering of wave functions and eigenenergies to the individual electrons of an atom. *Physica* **1933**, *1*, 104–113. [[CrossRef](#)]
42. Parr, R.G.; Yang, W. *Density-Functional Theory of Atoms and Molecules*; Oxford University Press: New York, NY, USA, 1989.
43. Parr, R.G.; Szentpaly, L.V.; Liu, S. Electrophilicity index. *J. Am. Chem. Soc.* **1999**, *121*, 1922–1924. [[CrossRef](#)]
44. Singh, R.N.; Kumar, A.; Tiwari, R.K.; Rawat, P.; Gupta, V.P. A combined experimental and quantum chemical (DFT and AIM) study on molecular structure, spectroscopic properties, NBO and multiple interaction analysis in a novel ethyl 4-[2-(carbamoyl) hydrazinylidene]-3, 5-dimethyl-1H-pyrrole-2-carboxylate and its dimer. *J. Mol. Struct.* **2013**, *1035*, 427–440. [[CrossRef](#)]

45. Hubert Joe, I.; Kostova, I.; Ravikumar, C.; Amalanathan, M.; Pinzaru, S.C. Theoretical and vibrational spectral investigation of sodium salt of acenocoumarol. *J. Raman Spectrosc.* **2009**, *40*, 1033–1038.
46. Sebastian, S.; Sundaraganesan, N. The spectroscopic (FT-IR, FT-IR gas phase, FT-Raman and UV) and NBO analysis of 4-Hydroxypiperidine by density functional method. *Spectrochim. Acta Part A Mol. Biomol. Spectrosc.* **2010**, *75*, 941–952. [[CrossRef](#)]



© 2020 by the authors. Licensee MDPI, Basel, Switzerland. This article is an open access article distributed under the terms and conditions of the Creative Commons Attribution (CC BY) license (<http://creativecommons.org/licenses/by/4.0/>).